JAMES | Journal of Advances in Modeling Earth Systems

RESEARCH ARTICLE
10.1029/2018MS001488

The Impact of Rimed Ice Hydrometeors on Global and Regional Climate

A. Gettelman[1], **H. Morrison**[1], **K. Thayer-Calder**[1], **and C. M. Zarzycki**[1]

[1]National Center for Atmospheric Research, Boulder, CO, USA

Key Points:
- Rimed hydrometeors (graupel or hail) are added to a stratiform cloud scheme for global models
- Global climate impacts are limited to small increases in ice mass
- High (14 km) resolution simulations show local production of rimed ice (graupel) can affect regional precipitation amounts and intensity

Correspondence to:
A. Gettelman,
andrew@ucar.edu

Citation:
Gettelman, A., Morrison, H., Thayer-Calder, K., & Zarzycki, C. M. (2019). The impact of rimed ice hydrometeors on global and regional climate. *Journal of Advances in Modeling Earth Systems*, *11*, 1543–1562. https://doi.org/10.1029/2018MS001488

Received 29 AUG 2018
Accepted 13 FEB 2019
Accepted article online 17 FEB 2019
Published online 6 JUN 2019

Abstract Rimed hydrometeors (graupel or hail) are added to a stratiform cloud scheme for global models and tested in a variety of configurations. Off-line tests compare well to other cloud microphysics schemes with rimed ice used in mesoscale models. Tests in single column and climate mode show expected production of small amounts of rimed ice in the middle troposphere and at high latitudes. The overall climate impacts of rimed ice (hail or graupel) at 100-km horizontal grid spacing are small. There are some changes to partitioning between cloud ice and snow that affect upper troposphere water budgets and clouds. High-resolution simulations are conducted with a global but regionally refined grid at 14 km over the Contiguous United States. High-resolution simulations show local production of graupel with realistic size and number concentrations. The maximum graupel frequency at high resolution is over Western U.S. mountain ranges. Differences in total precipitation with the addition of rimed ice in 8-year simulations are statistically significant only for orographic precipitation over the Cascade and Rocky mountains, reducing model biases when rimed ice is included. Rimed ice slightly improves summer precipitation intensity relative to observations. Thus, while the global climate impact of rimed ice in stratiform clouds may be negligible, there are potentially important and systematic regional effects, particularly for orographic precipitation. Rimed ice in cumulus clouds is not yet treated but is an important next step.

Plain Language Summary Rimed ice, known commonly as graupel or hail, forms with higher velocity updrafts in clouds, often convective clouds. These updrafts are usually not present for low-resolution global models used for climate. But graupel and hail are important for simulating the evolution of precipitation correctly. This work describes implementation of graupel and hail into a global climate model, with tests using a suite of models from idealized updrafts up to regional climate experiments with 14-km resolution. The new cloud physics scheme produces reasonable amounts of graupel especially at regional climate scales. There are few impacts on the simulations, but some shifts in precipitation result. This paper is an important foundation for higher-resolution global models.

1. Introduction

Significant production of rimed hydrometeors (graupel and/or hail) at the grid scale requires vertical velocities much higher than would be expected or reasonable at scales of 100 km typical of global climate models. That is why global climate models typically forego the representation of rimed ice. However, increases in computational power have allowed global models to simulate features at higher resolution, and new methods for variable mesh simulations have enabled regional climate modeling at resolutions more typical of mesoscale models (10–25 km; e.g., Gettelman et al., 2018; Huang et al., 2016; Rauscher et al., 2012; Zarzycki & Jablonowski, 2014). There are also ongoing efforts at unification of weather and climate models (Brown et al., 2012). The overall requirement of these efforts is physical parameterizations which can appropriately represent the state of the atmosphere across a wide range of scales (often called "scale-insensitive" parameterizations). The goal is to develop a parameterization that responds appropriately to the forcing at any grid resolution without modification or tuning.

Representing rimed ice is important as resolution increases in models. Smaller scales with larger updraft velocities are resolved, and these can produce rimed ice. Representation of rimed ice has been shown to be important for mesoscale modeling of several different regimes, including frontal rainbands (Rutledge & Hobbs, 1984) and deep convective systems (Adams-Selin et al., 2013; Bryan & Morrison, 2012; McCumber et al., 1991; van den Heever & Cotton, 2004; Van Weverberg et al., 2012; Wu et al., 2013). Rimed ice is

important for simulating some cases of winter orographic precipitation (Colle et al., 2005, 2008; Lin et al., 2011; Morrison et al., 2015).

For cloud microphysics schemes used for large-scale (stratiform) clouds, there has been a convergence of methods. Advanced two-moment microphysics schemes that predict mass and number of cloud drops exist for both mesoscale models (Ferrier, 1994; Lim & Hong, 2010; Milbrandt & Yau, 2005; Morrison et al., 2009; Seifert & Beheng, 2006; Thompson et al., 2008) and for climate models (Gettelman et al., 2015; Lohmann et al., 1999). A key difference remaining between these schemes is the representation of rimed hydrometeors (hail or graupel). Because of the lack of strong resolved scale updrafts, large-scale climate models typically do not explicitly treat rimed hydrometeors. However, high-resolution global models are able to generate these motions, and so representation of rimed ice may be important for global applications. Lin and Colle (2011) parameterized ice fall speeds in a General Circulation Model (GCM) to account for the effects of riming and found 20–30% increases in upper tropospheric ice, with ~1 Wm^{-2} change in the global radiative balance, indicating the potential for significant climate impacts.

The purpose of this paper is to document the extension of a stratiform cloud microphysics scheme for global models of climate and weather events to include an explicit treatment of rimed ice. We do this using a model hierarchy that tests the scheme over a wide range of conditions from weak grid scale forcing at 100 km, to explicit mesoscale forcing at 14 km, to stronger forcing representing deep convective updrafts. The scheme is run first in an off-line model and compared to typical schemes for mesoscale and cloud models with a cloud scale deep convective updraft. Next we examine key processes in a single column framework with large-scale forcing representative of 100-km scales. Finally, the new scheme is run for global climate (100-km scales) and regionally refined high-resolution simulations (14 km, partially resolved convective scales). Large-scale differences in climate are not expected, but regional impacts may result at higher resolution. We discuss extensions of such an approach to convective clouds in the conclusions (section 7).

This manuscript is organized as follows. Section 2 describes the adjustments to the scheme to represent rimed ice. Section 3 presents off-line tests with a Kinematic Driver (KiD; Shipway & Hill, 2012). Section 4 illustrates process rates from single column tests. Section 5 presents global results from 1° simulations with the Community Atmosphere Model version 6 (CAM6), and section 6 presents results from CAM6 refined mesh simulations over the Contiguous United States (CONUS). Conclusions and future work are in section 7.

2. Scheme Description

We have developed a third version of the scheme originally described by Morrison and Gettelman (2008), termed "MG." A version with prognostic rain and snow and performance improvements was developed by Gettelman and Morrison (2015), called "MG2." Here we describe the implementation of rimed hydrometeors in the scheme, hereafter "MG3." We will focus on the differences between MG2 and MG3 and between MG3 and other microphysics schemes that treat rimed hydrometeors.

The addition of rimed ice in MG3 follows the treatment in the Morrison et al. (2009) mesoscale microphysics scheme. A schematic of the MG3 scheme is shown in Figure 1. MG3 starts with MG2 (Gettelman & Morrison, 2015) and adds a series of processes (in red). One rimed hydrometeor category is added. Both mass and number are prognosed. Rimed ice has the "character" of hail or graupel by preselecting density and fall speed parameters as described below.

The conservation equation for the mass mixing ratio of rimed ice is given as

$$\begin{aligned}\frac{dQ_G}{dt} =& Q_{G\text{sed}} + Q_{G\text{adv}} + Q_{G\text{dif}} + \\ & (PRACG + PGRACS + PRDG + PSACR + MNUCCR) f_p + \\ & (PSACWG + PGSACW) f_c, \end{aligned} \quad (1)$$

where G refers to the rimed ice category (graupel or hail), and then Q_G is the graupel/hail mass mixing ratio. Q_G tendencies due to sedimentation ($Q_{G\text{sed}}$), advection ($Q_{G\text{adv}}$) and diffusion ($Q_{G\text{dif}}$) are also included. f_p is the precipitation fraction, f_c is the cloud fraction, and the various process rates are defined in Table 1. Note that precipitation fraction is always equal to or greater than cloud fraction at a given level. MNUCCR is the freezing of rain to rimed ice (see Appendix A).

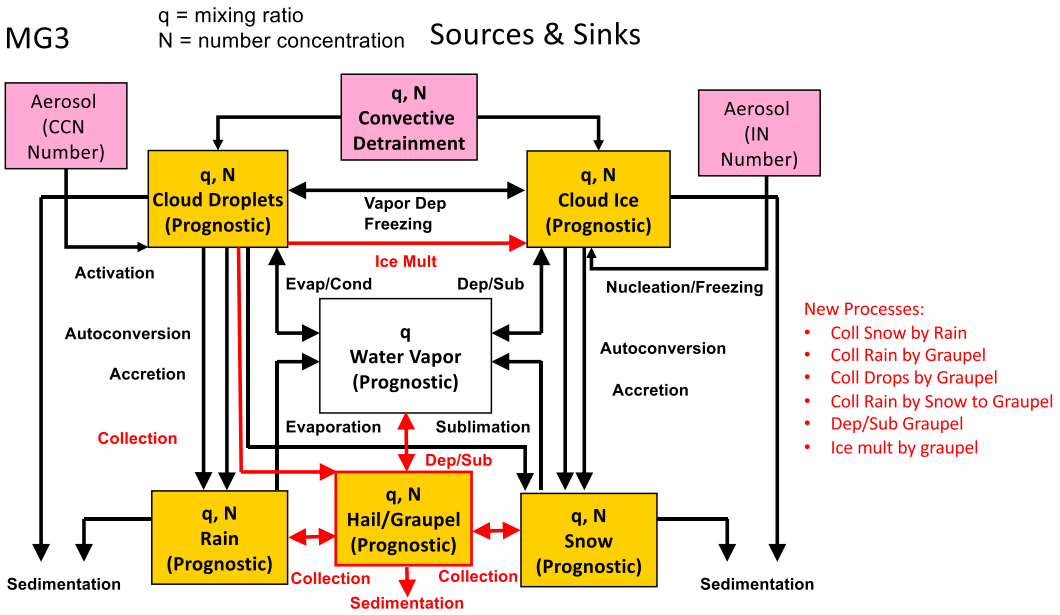

Figure 1. Schematic of the stratiform cloud microphysics scheme. New rimed ice processes are shown in red.

The equation for rimed ice number mixing ratio is

$$\frac{dN_G}{dt} = N_{G\text{sed}} + N_{G\text{adv}} + N_{G\text{dif}} + (NSCNG)f_c + (NGRACS + NNUCCR)f_p, \quad (2)$$

where N_G is the rimed ice number mixing ratio. N tendencies due to sedimentation ($N_{G\text{sed}}$), advection ($N_{G\text{adv}}$), and diffusion ($N_{G\text{dif}}$) are also included. The different process rates are defined in Table 1. NNUCCR is the freezing of rain to rimed ice (Appendix A).

Inclusion of rimed ice also requires changes to the existing equations for the evolution of vapor (Q_v), cloud droplets (Q_c, N_c), cloud ice (Q_i, N_i), rain (Q_r, N_r), and snow (Q_s, N_s). These changes are detailed in Appendix A.

Rimed ice particles are assumed to follow an inverse exponential distribution, as defined in Morrison and Gettelman (2008, Equations 1–4). The overall treatment in Morrison et al. (2009) follows Reisner et al. (1998), Murakami (1990), and Ikawa and Saito (1990). Deposition or sublimation of rimed ice (PRDG) is treated similarly to evaporation of rain or snow (Morrison et al., 2005, eqs. 3 and 8). Collection of snow by rain to form rimed ice (PSACR) follows Reisner et al. (1998), Equation A.47, and is defined as

$$PSACR = \pi^2 \rho_s \epsilon(((1.2U_{\text{Rm}} - 0.95U_{\text{Sm}})^2 + 0.08U_{\text{Sm}}U_{\text{Rm}})^{0.5} \rho N_{0r} N_{0s} / \lambda_s^3 * (5/(\lambda_s^3\lambda_r) + 2/(\lambda_s^2\lambda_r^2) + 0.5/(\lambda_s\lambda_r^3))), \quad (3)$$

Table 1
New Microphysical Processes for Rimed Ice

Q Process	N Process	Description
PSACR		Collection of snow by rain
PRACG	NPRACG	Collection of rain by graupel/hail
PSACWG	NPSACWG	Collection cloud water by graupel/hail
PGSACW	NSCNG	Conversion of rimed cloud water to graupel/hail
PGRACS	NGRACS	Conversion of rain rimed onto snow to graupel/hail
PRDG		Graupel deposition/sublimation
QMULTG	NMULTG	Rime splintering (ice multiplication) from cloud water
QMULTRG	NMULTRG	Rime splintering of accreted rain

where ρ_s is the density of snow, $\epsilon = 1$ is the collection efficiency, U_{Rm} and U_{Sm} are the mass weighted rain and snow mass fall speeds, respectively, N_{0r} and N_{0s} are the intercept parameters for rain and snow, and λ_r and λ_s are the slope parameters for rain and snow (see Morrison & Gettelman, 2008). ρ is the air density.

Collection of rain by rimed ice (PRACG,NPRACG) follows a similar form (Reisner et al., 1998, equation A.48):

$$PRACG = \pi^2 \rho_w \epsilon_r (((1.2U_{\mathrm{Rm}} - 0.95U_{\mathrm{Gm}})^2 + 0.08U_{\mathrm{Gm}}U_{\mathrm{Rm}})^{0.5} \rho N_{0r} N_{0g} / \lambda_r^3 (5/(\lambda_r^3 \lambda_g) + 2/(\lambda_g^2 \lambda_r^2) + 0.5/(\lambda_s \lambda_g^3))), \quad (4)$$

$$NPRACG = \pi/2 \rho_w \epsilon_r (1.7(U_{\mathrm{Rn}} - U_{\mathrm{Gn}})^2 + 0.3U_{\mathrm{Gn}}U_{\mathrm{Rn}})^{0.5} N_{0r} N_{0g} (1/(\lambda_r^3 \lambda_g) + 1/(\lambda_r^2 \lambda_g^2) + 1/(\lambda_g^3 \lambda_r)), \quad (5)$$

where $\epsilon_r = 1$ is the rain collection efficiency. U_{Gm} is the mass weighted fall speed for graupel mass (see equation (10)). Mass weighted fall speeds for number are U_{Rn} for rain, U_{Sn} for snow, and U_{Gn} for graupel (equation (11)).

Collection of cloud water by rimed ice (PSACWG,NPSACWG) is defined as (equation A.61, Reisner et al., 1998):

$$PSACWG = \Gamma(b+3)(\pi/4)\epsilon_{\mathrm{id}} a q_c \rho N_{0g} / \lambda_g^{(b+3)}, \quad (6)$$

$$NPSACWG = \Gamma(b+3)(\pi/4)\epsilon_{\mathrm{id}} a N_c \rho N_{0g} / \lambda_g^{(b+3)}, \quad (7)$$

where a and b are shape parameters for fall speed set differently for hail and graupel (see below). ϵ_{id} is the ice-droplet collision efficiency. N_{0g} and λ_g are the intercept and slope parameters for rimed ice.

Conversion of rimed cloud water to rimed ice (PGSACW,NSCNG) follows Reisner et al. (1998, equation A.43; originally Ikawa & Saito, 1990) and only occurs when $q_s > 0.1$ g/kg and $q_c > 0.5$ g/kg, where q_s is the in-cloud snow mixing ratio and q_c is the in-cloud liquid mixing ratio, following Rutledge and Hobbs (1984).

Conversion of rain collected by snow into rimed ice (PGRACS,NGRACS) follows Reisner et al. (1998, equations A.50 and A.51) and uses the threshold values for the conversion of $q_s > 0.1$ g/kg and $q_r > 0.1$ g/kg, where q_s is the in-cloud snow mixing ratio and q_r is the in-cloud rain mixing ratio, following Rutledge and Hobbs (1984). This modifies snow as well (PRACS,PSACR; see appendix A).

Rime splintering or ice multiplication from cloud water (QMULTG,NMULTG) and riming and splintering from accreted raindrops (QMULTRG,QMULTRG) occur from −8 to −3 °C, following

$$NMULTG = f 3.5 \times 10^8 PSACWG, \quad (8)$$

where f is a triangular function ramped from 0 at −3 °C to $f = 1$ at −5 °C and then back to 0 at −8 °C. QMULTG = NMULTG * M_{g0}, where M_{g0} is the mass of an ice splinter (ice, 10 microns diameter). QMULTG is constrained so that transfer of mass from rimed ice to cloud ice cannot be more mass than was rimed (QMULTG < PSACWG), and PSACWG is reduced as a result. Finally, splintering associated with accreted raindrops (QMULTRG, NMULTRG) is calculated similarly:

$$NMULTRG = f 3.5x10^8 PRACG, \quad (9)$$

and QMULTRG = NMULTRG * M_{g0}, constrained by the mass transfer from rain to graupel.

Following Morrison and Gettelman (2008), the fall speeds (U_G) for rimed hydrometeors are specified by a diameter-fall speed relationship $U = aD^b$ for a particle with diameter D. The mass weighted fall speed (m/s) is found by integrating over the size distribution:

$$U_{\mathrm{Gm}} = min(a\Gamma(4+b)/(6\lambda_g^b), 20)(\rho_0/\rho)^{0.54}. \quad (10)$$

Similarly, the number weighted fall speed (m/s) is

$$U_{\mathrm{Gn}} = min(a\Gamma(1+b)/(\lambda_g^b), 20)(\rho_0/\rho)^{0.54}, \quad (11)$$

where λ_g is the rimed ice shape parameter. ρ_0 is a reference air density at 850 hPa, and ρ is the air density. The last term is an air speed correction factor (units of m/s) from Heymsfield et al. (2007). U_{Gm} and U_{Gn} are used to derive the sedimentation tendencies ($Q_{G\mathrm{sed}}, N_{G\mathrm{sed}}$) in equations (1) and (2) using a first-order upwind flux difference (Gettelman & Morrison, 2015).

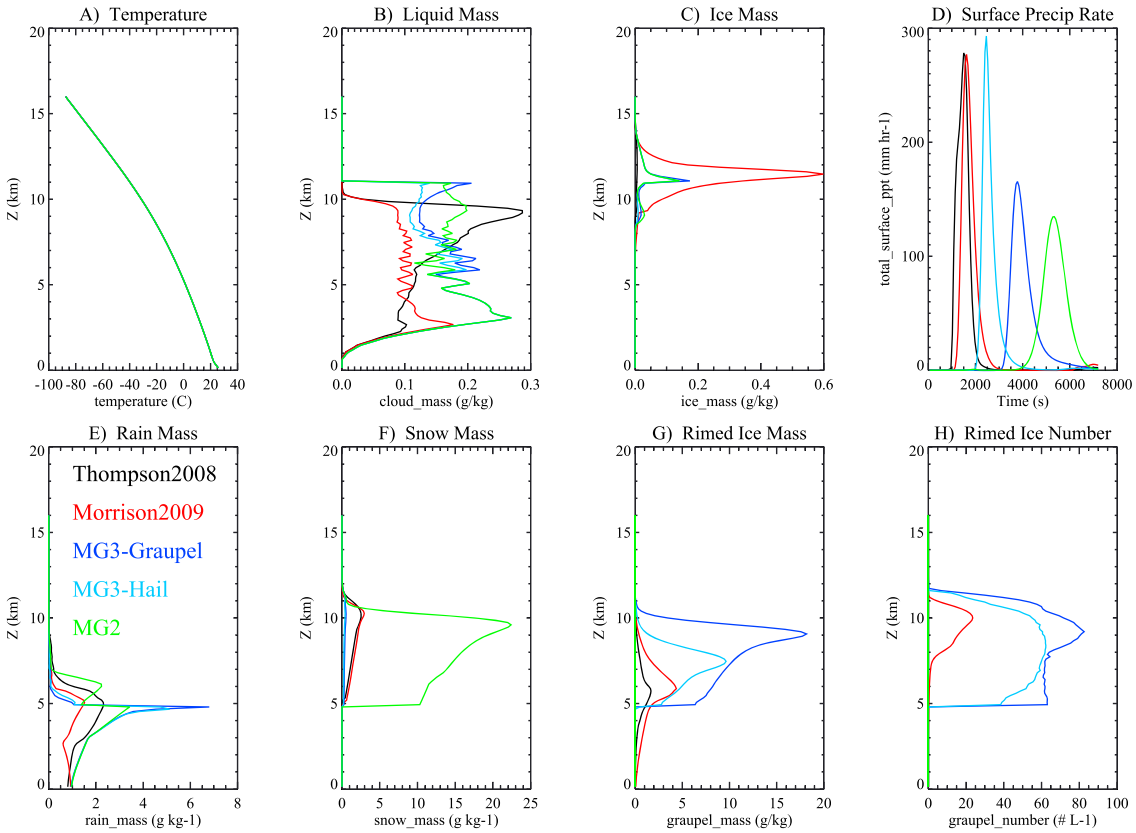

Figure 2. Time average of a Kinematic Driver transient deep convective simulation with several different microphysics schemes: MG3 with hail-cyan, MG3 with graupel-blue, M2009-red, T2008-black, and MG2-green.

There is a switch in the code to change between graupel and hail, with the only difference being the bulk density and the fall speed-size relationship. For graupel, $\rho_g = 500 \text{kgm}^{-3}$, and for hail, $\rho_h = 900 \text{kgm}^{-3}$. For graupel, a = 19.3 $\text{m}^{1-b}\text{s}^{-1}$ and b = 0.37 (unitless; Locatelli & Hobbs, 1974). For hail, a = 114.5 and b = 0.5 (Matson & Huggins, 1980).

We designed the MG3 scheme with the goal to develop a parameterization that can work across scales. In the case of the KiD 1-D and single column model tests, hail parameters might be appropriate for the updraft speeds, and so we test with hail and graupel parameters there. In the GCM tests down to 14 km in this work, updraft speeds are more appropriate for graupel (see below), so we have just shown simulations with graupel parameters. The goal is to provide options, even if most current global model applications will use parameters associated with graupel.

3. KiD Tests

For testing, MG3 is implemented in the KiD (Shipway & Hill, 2012). Also available in the KiD model for comparison are the base MG2 scheme, (Gettelman & Morrison, 2015), the Morrison et al. (2009) scheme based on Morrison et al. (2005; hereafter M2009), and the Thompson et al. (2008) scheme (hereafter T2008). Note that KiD has a cloud fraction of either 0 or 1. The MG scheme (all versions) has a switch to assume uniform grid box properties that is used in the KiD tests. All the microphysics schemes in KiD are running with essentially the same forcing, binary (0 or 1) cloud fraction, and uniform grid box properties.

Here we analyze the transient deep convective KiD case (Case 11 in Shipway & Hill, 2011) with an updraft that decays in time and height applied to hydrometeors and vapor. The maximum updraft strength is 16 m/s. This updraft strength is typical of moderate deep convection and would represent a small scale (Large Eddy Simulation or Cloud Resolving Model type) model of deep convection. The simulation is 2 hr (7,200 s) long. The profiles of temperature and moisture are those described by Shipway and Abel (2010). Temperature is

Table 2
Kinematic Driver Simulation Precipitation

Simulation	Mean LWP (kg/m^2)	Avg Precip ($kg \cdot m^{-2} \cdot s^{-1}$)
T2008	0.735	23.61
M2009	0.594	23.77
MG3-Graupel	1.042	21.52
MG3-Hail	0.989	21.89
MG2	1.057	21.95

kept fixed to minimize microphysical feedback. A source term for vapor is applied, and the updraft decays over time. Details are described in Shipway and Hill (2011).

Figure 2 illustrates a KiD simulation with MG3 for the deep convective case. The figures are time averages of the cloud over the whole simulation, with the evolution of precipitation shown in Figure 2d. The key aspects of this case are to compare the MG3 implementation to MG2 and to other similar microphysical schemes with a rimed ice hydrometeor category. Figure 2 illustrates MG3 simulations with graupel (dark blue, dotted) and hail (cyan, dot dash) as well as MG2 (the same scheme without graupel and hail, green solid), M2009 (purple solid), and T2008 (black solid) microphysics schemes. All the schemes have fixed drop number of 100 cm^{-3} and ice nucleation following Cooper (1986).

MG3 gives results comparable to the other schemes, with a similar vertical rain structure (Figure 2e) and temporal evolution (Figure 2d). There is more liquid water in the MG2 and MG3 schemes than in the other schemes, particularly lower in the cloud (Figure 2b). This is illustrated in Table 2, where there is ~30–40% higher Liquid Water Path (LWP) in MG2 and MG3 than in M2009 and ~25% more than T2008. Note that MG2 and MG3 have nearly the same cloud liquid below the melting level. The MG3 scheme with hail gives a slightly delayed timing of precipitation compared to T2008 and M2009 (Figure 2d). The M2009 simulation specifies rimed ice properties as hail. When using graupel properties instead in MG3, it produces more mass and number of rimed ice (Figures 2g and 2h) and a larger delay in the timing of precipitation. Average precipitation is ~10% higher with T2008 and M2009 than with MG3 (Table 2). MG3 produces an order of magnitude more graupel mass than T2008 and a factor of 3 larger than M2009 (Figure 2g), largely due to the large snow mass in MG2.

The main difference between MG2 (no graupel/hail) and MG3 with either graupel or hail is a large reduction in snow above the melting level at 5 km in the simulations, which is associated with generation and growth of rimed ice in MG3. This transformation also significantly impacts the timing of precipitation, as snow has a much slower mass-weighted mean fall speed (1–2 ms^{-1}) than hail or graupel (up to 5–10 ms^{-1} in these simulations). Consequently, MG2 has substantially delayed precipitation relative to all of the schemes that explicitly treat rimed ice (MG3, T2008, and M2009).

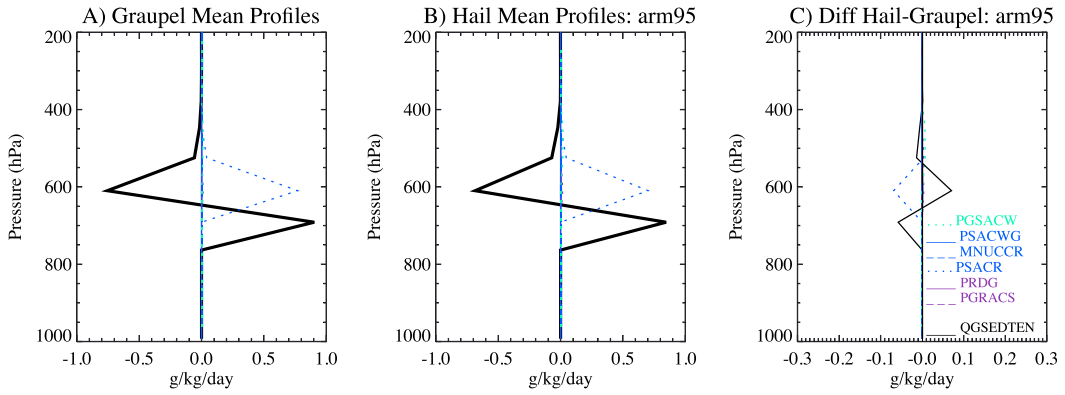

Figure 3. Average graupel tendency profiles for the ARM summer 1995 deep convective case. (a) Simulation with graupel. (b) Simulation with hail. (c) Difference hail-graupel. Tendencies are as in Table 1.

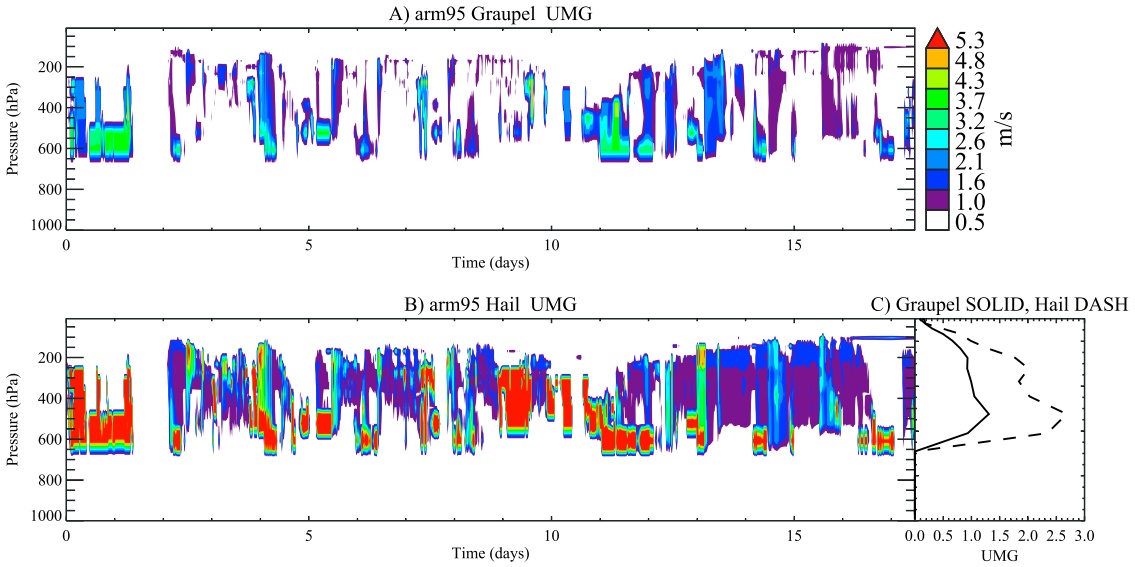

Figure 4. Rimed ice mass weighted mean fall speed (UMG) in meter per second for the ARM summer 1995 case using parameters for (a) graupel and (b) hail (bottom). (c) shows the time mean (graupel solid, hail dashed).

4. Single Column Results

To perform single column and global simulations, the MG3 scheme is implemented in the CAM6, the atmospheric component of the Community Earth System Model version 2. MG3 is set up to simulate either graupel or hail by selecting a density of the rimed hydrometeors and different fall speed parameters as described above.

CAM6 features a two-moment stratiform cloud microphysics scheme (MG2), that is coupled to a unified moist turbulence scheme, Cloud Layers Unified by Binormals (CLUBB), developed by Golaz et al. (2002) and Larson et al. (2002) and implemented in CAM by Bogenschutz et al. (2013). CLUBB handles stratiform clouds, boundary layer moist turbulence, and shallow convective motions. The two-moment cloud microphysics for MG2 and MG3 is implemented in this version, and all of the CLUBB-simulated cloud types are potential sources for rimed ice. CAM6 also has an ensemble plume mass flux deep convection scheme described by Zhang and McFarlane (1995), which has very simple microphysics. Thus, we are not treating rimed ice associated with parameterized deep convection in the global model. Note that a deep convective case was tested in section 3 using an off-line KiD.

First, we use the Single Column Atmosphere Model (SCAM) in CAM6 (Gettelman et al., 2019) to simulate single column cases. These cases run the full suite of CAM6 physics parameterizations but with constrained meteorology. We relax horizontal wind and temperature to a specified forcing. We have explored stratiform mixed phase cases such as the Mixed Phase Arctic Cloud Experiment as well as continental cases over the

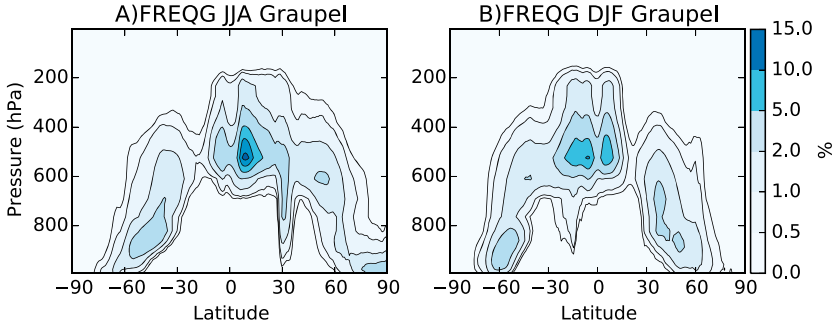

Figure 5. Zonal mean FREQG from a global simulation. (a) JJA and (b) DJF. FREQG = frequency of occurrence of graupel; JJA = June–August; DJF = December–February.

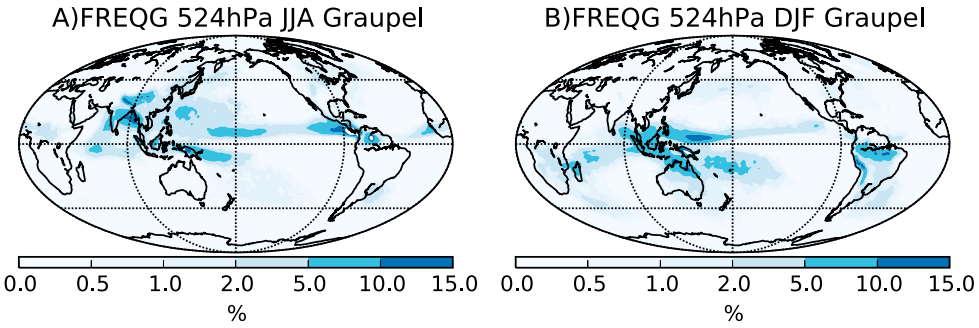

Figure 6. FREQG from a global simulation at 524 hPa. (a) JJA and (b) DJF. FREQG = frequency of occurrence of graupel; JJA = June–August; DJF = December–February.

Atmospheric Radiation Measurement (ARM) Southern Great Plains site (see below) and oceanic convective cases such as the Tropical Ocean Global Atmosphere case. Averages of water path and top of atmosphere fluxes for MG2 and MG3 vary slightly but not systematically between cases (not shown), though LWP is a few percent lower in the convective cases with MG3 than MG2, consistent with KiD results in Table 2. In the convective cases, a small mass of graupel and hail is present above the melting level. Note that in SCAM, there is a diagnostic deep convective scheme active, with no rimed ice, and MG3 treats rimed ice in stratiform updrafts that are a maximum of 2–10 cm^{-1}. Rimed ice in MG3 in SCAM is more typical to that in a global simulation at 100-km resolution.

Figure 3 illustrates the average tendencies for a continental case at the DOE ARM Southern Great Plains Site from 18 July to 4 August 1995. The dominant graupel production process is collection of snow by rain (PSACR, Table 1). This is slightly larger at higher altitudes when rimed ice is graupel (Figure 3a) compared to hail (Figure 3b). There is a small source term for the collection of rain by graupel/hail (PRACG), and for graupel, there is an additional small source due to collection of cloud liquid by graupel (PSACWG). Sedimentation is an important sink for graupel and hail, as is melting (not shown).

Figure 4 shows the difference in mass weighted mean fall speed (UMG) between graupel (top) and hail (bottom). Hail fall speeds are up to 5 ms^{-1}, with a time mean that is double that of graupel (2 vs. 1 ms^{-1}). In general, the mass of graupel is larger than the mass of hail, but it falls slower.

5. Global Results

Next we present results using MG3 with settings for graupel implemented in CAM6. Simulations are run at 1° (~100 km) horizontal resolution with climatological Sea Surface Temperatures (SSTs) representing the 1990–2000 time period. The first year of simulations are not analyzed, and the next 9 years are averaged to develop a climatology.

At 100-km horizontal resolution, there is very little graupel in the simulations (generally just a few parts per million by mass). Figure 5 illustrates the zonal mean climatological FREQG for June–August (JJA, Figure 5a)

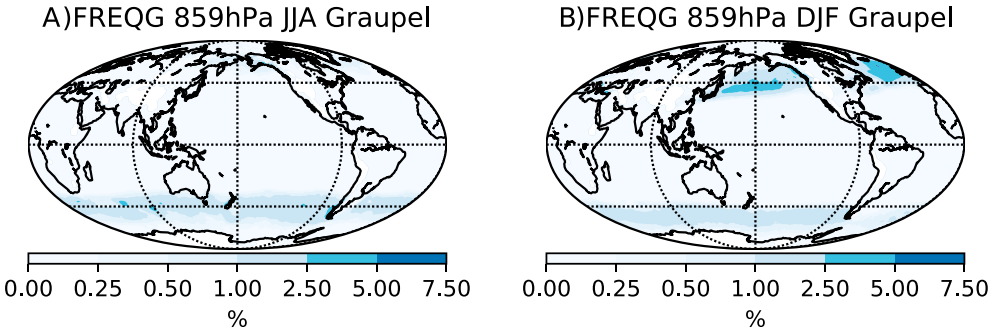

Figure 7. FREQG from a global simulation at 859 hPa. (a) JJA and (b) DJF. Areas below ground level at 859 hPa masked white. FREQG = frequency of occurrence of graupel; JJA = June–August; DJF = December–February.

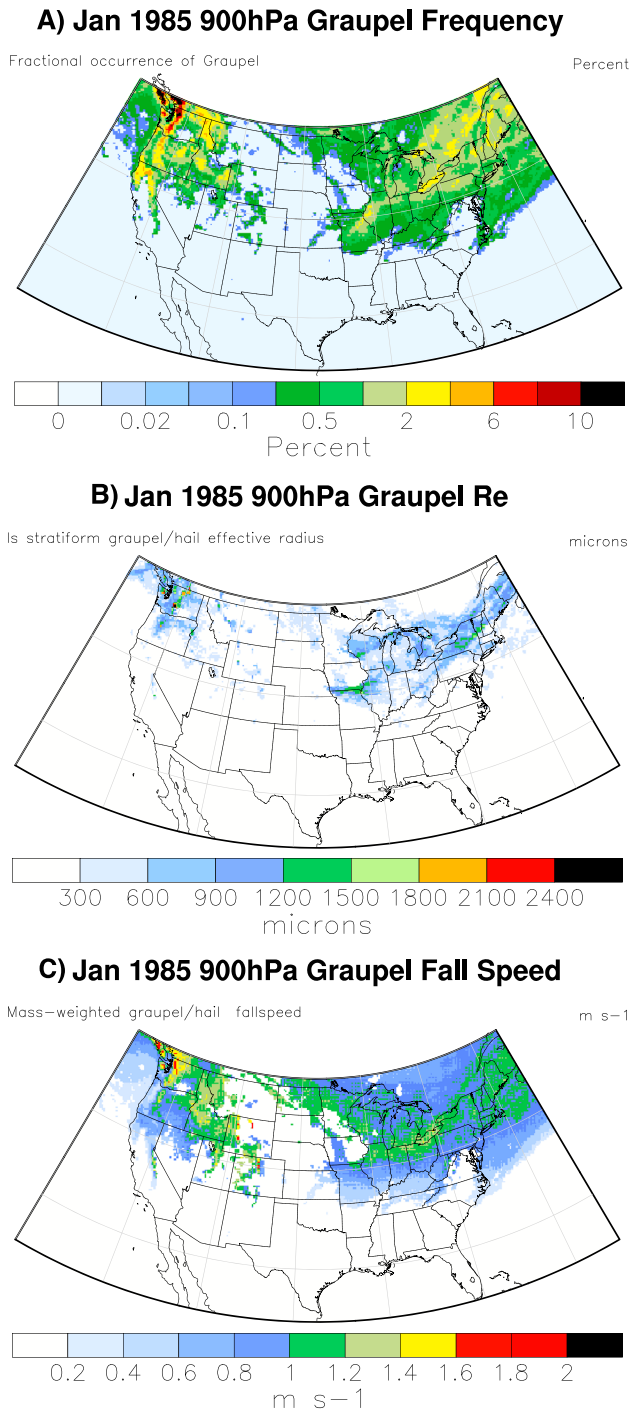

Figure 8. January 1985 900-hPa Graupel 14-km simulation mean (a) frequency, (b) effective radius (Re), (c) mass-weighted fall speed.

and December–February (Figure 5b). Graupel occurrence frequency is calculated as the fractional coverage of precipitation when the mass mixing ratio is larger than 10^{-7} kg/kg (0.1 ppmm) at each time step and averaged across time steps. If there is less graupel mass than this, the frequency in a time step is zero. The peak occurrence is about 550 hPa in the tropics at just over 10%. There are secondary peaks in the midlatitude storm tracks at lower altitude.

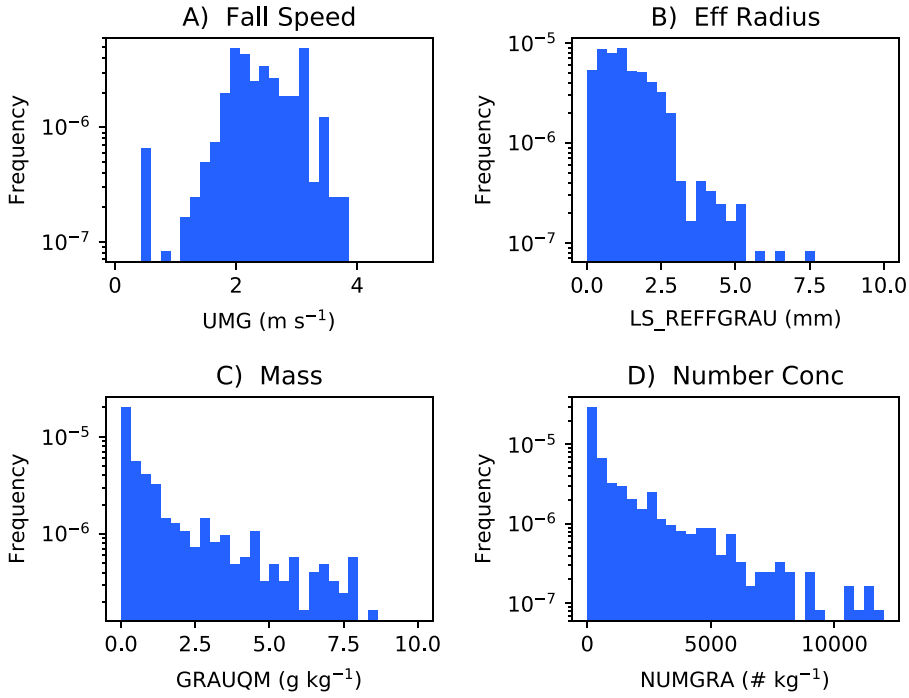

Figure 9. January 1985 lower troposphere (990–850 hPa) normalized probability distributions for Contiguous United States of (a) mean mass weighted graupel fall speed (UMG, m/s), (b) graupel effective radius (LS_REFFGRAU, mm), (c) graupel mass mixing ratio (GRAUQM, g/kg) and (d) graupel number mixing ratio (NUMGRAU, # per kilogram).

The distribution of graupel is different in the tropics (Figure 6) and midlatitudes (Figure 7). In the tropics (Figure 6), graupel is found in regions with deep convection and peaks at about 550 hPa in the summer hemisphere tropics and subtropics. Note that rimed ice is not being produced within the deep convective scheme itself but is a product of large-scale grid-resolved motion and indirectly from the evolution of convectively detrained hydometeors (convection only detrains cloud liquid and cloud ice).

In midlatitudes (Figure 7), the frequency of occurrence is lower (note that the scale is half that of Figure 6) and closer to the surface, peaking at ~850 hPa. In the North Hemisphere, it peaks in winter in the oceanic storm tracks, while in the South Hemisphere, features are more constant throughout the year, with a slight peak in winter. The peak is over the ocean, where more stratiform liquid water occurs.

The small graupel mass limits any "climate" impact. Globally, there is a small (0.3 gm^{-2} or 2%) increase in ice water path (IWP: suspended ice only, not including snow) in the simulation with graupel compared to the MG2 control, mostly confined to tropical convective regions. The IWP change is associated with slightly higher upper-tropospheric cloud cover. There is no significant radiative effect of this small IWP change. In addition, there is a small decrease in snow. These effects are consistent with the formation of rimed ice, growth by riming, as well as faster fall speeds of graupel than snow. They are also consistent with the single column simulations in Figure 3 that showed the dominant graupel production process is collection of snow by rain (and faster fall speeds than snow), hence explaining the reduction in snow mass.

These results show smaller impacts than Lin and Colle (2011), who reported a 10–20% increase in ice mass by parameterizing rimed ice fall speeds. Lin and Colle (2011) used rimed ice fall speeds that were faster than ice fall speeds used in their GCM but slower fall speeds than the typical empirical parameterization (Heymsfield & Donner, 1990). The mechanism is quite different than the GCM studies here, however, as this work treats rimed ice with multiple processes and interactions with hydrometeors, not just modifications to the fall speed. Thus, we do not expect comparable results, and the lack of a large signal indicates microphysical processes other than sedimentation are important for rimed ice effects.

Overall, as expected, there is little climate significance to the addition of rimed ice in these 1° horizontal resolution simulations.

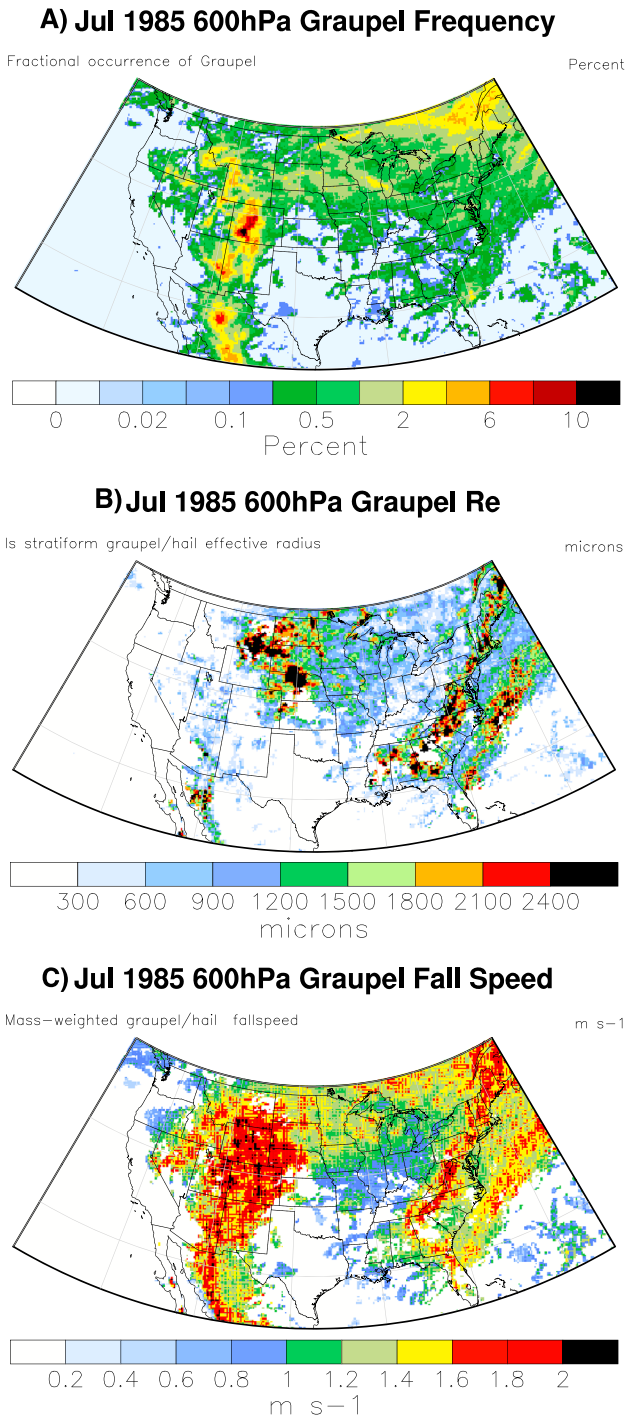

Figure 10. July 1983 600-hPa graupel 14-km simulation (a) frequency, (b) effective radius (Re), and (c) fall speed.

6. Refined Mesh Simulations

To examine the performance of MG3 at higher horizontal resolution, where rimed ice is expected to be more important than in a ~10-km model, we also perform simulations with CAM6 using a variable-resolution mesh. The atmosphere model uses the Spectral Element dynamical core (Taylor, 2011), with the variable-resolution configuration described in Zarzycki et al. (2014). A refined mesh down to 14-km horizontal resolution is generated with SQuadGen (Guba et al., 2014), focused over the CONUS. The approximate region of high resolution is shown in Figure 8. The background global resolution is approximately 111

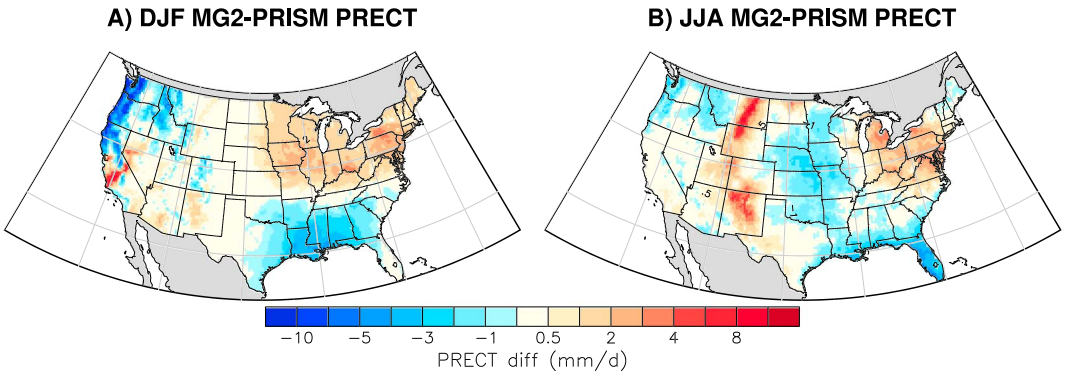

Figure 11. Difference between MG2 and PRISM precipitation data set based on daily 12-km data for (a) DJF and (b) JJA. DJF = December–February; JJA = June–August; PRISM = Parameter-elevation Relationships on Independent Slopes Model.

km, with two intermediate transition regions between the highest and lowest resolutions. All elements use the same time step, regardless of resolution. The global physics time step is set to 600 s. Explicit diffusion in the Spectral Element dynamical core is scaled as in Guba et al. (2014), with local diffusion coefficients matching CAM defaults for the corresponding uniform resolution configurations. The refined mesh runs at 6% of the cost of a globally uniform 14-km mesh due to the reduced number of global elements.

Simulations are run for 8 years with observed SSTs for 1985–1992 (inclusive). One simulation was run with MG3 and rimed ice parameters corresponding to graupel, and one simulation was run with MG2 and no rimed ice hydrometeors. All other parameters were the same in the simulations.

Figures 8 and 10 illustrate a single month mean from the simulations, indicating the mean frequency, size (effective radius, Re), and mass-weighted fall speed. Figure 8 at 900 hPa is "near surface" in the terrain following hybrid coordinate. Because MG3 uses a fixed density and a fixed size distribution shape, increases in effective radius are always associated with increases in mean fall speed—they are both inversely proportional to lambda. So from instantaneous data, the effective radius must increase with lambda (verified using the data in Figure 9), but this does not have to be true for monthly averaged data. In winter (Figure 8) graupel occurs close to the ground similar to the global uniform run (Figure 5b), with a peak near 900 hPa, while in summer (Figure 10), the peak is higher at around 600 hPa, similar to the global uniform simulations (Figure 5a) between 40° and 50° N.

At higher resolution, several additional features stand out compared to the low-resolution simulations. Figure 8 indicates peak graupel occurrence in January in regions of orographic precipitation in the Western United States. Mean sizes are on the order of 1-mm (1,000 microns) radius, and mean mass-weighted fall speeds can reach 1.5–2 ms^{-1}. Note that these are monthly averages.

Figure 9 shows probability distribution functions of instantaneous values over the high-resolution CONUS mesh during January 1985 between 990 and 850 hPa. Values may differ from Figure 8 due to removal of no graupel points in space and time. Figure 9 is constrained for $N_g > 2$ kg^{-1}, to remove a small fraction of cases when $N_g = 1$ kg^{-1}. Fall speeds are distributed around a mode of ~2.5 m/s, with maxima up to 4 m/s (Figure 9a). The peak instantaneous mean sizes can reach up to 5–7.5 mm in radius in the simulations (Figure 9b). The graupel mass is small, with occasional masses up to 5–10 g/kg (Figure 9c). The low-resolution (100 km) simulations are consistent with these distributions: At 100-km resolution, no graupel mass larger than 2 g/kg is produced, and fall speeds are less than 2 m/s. These values are outliers, with more typical values of graupel mass in the lowest bin of Figure 9c, with a mass less than 0.3 g/kg. This is consistent with KiD simulations indicating a larger graupel mass than other schemes (Figure 2g) and occurs because of large snow mass converted to graupel. Number concentrations of graupel are up to 10 L^{-1} (Figure 9d). Statistics for just the Western United States are similar.

In summer (Figure 10), the patterns are significantly different, reflecting the different seasonal character of precipitation and temperature regimes. Graupel occurs at higher altitudes and rarely reaches the surface: There is virtually no graupel at 900 hPa. Graupel occurrence peaks at ~600 hPa over a broad region of CONUS (Figure 10). There are high frequencies over the higher elevations of the Colorado plateau. Average

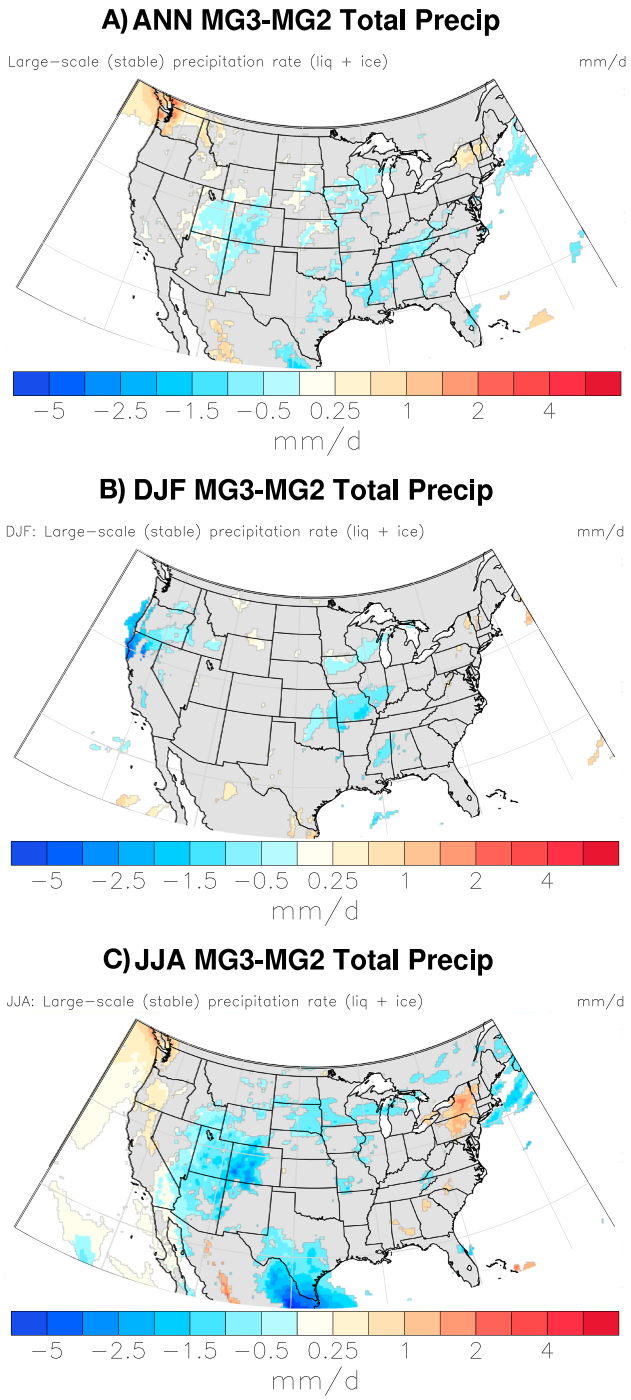

Figure 12. Difference in total (stratiform + convective) precipitation rate between MG3 and MG2 simulations. Only significant differences (see text) are shown. (a) ANN, (b) DJF, and (c) JJA. ANN = annual; DJF = December–February; JJA = June–August.

graupel sizes are larger than in winter (average radius up to 2.4 mm), with higher average fall speeds (up to 2 m/s). The seasonal shift still places maximum frequency of occurrence over mountain ranges, where resolved scale updrafts are the largest.

To further analyze differences between MG3 and MG2 simulations, daily averaged precipitation rate has been compared to the Parameter-elevation Relationships on Independent Slopes Model (PRISM) data set from the PRISM Climate Group, Oregon State University. The PRISM daily precipitation data set for the

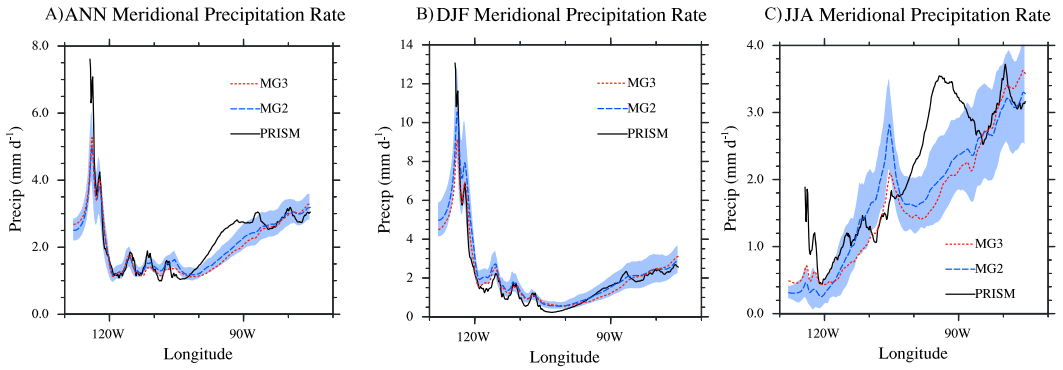

Figure 13. Seasonal precipitation rate averaged meridionally along a longitude strip from 38–48° N for PRISM observations (black-solid), MG2 (blue-dash), and MG3 (red-dotted). (a) ANN, (b) DJF, and (c) JJA. Blue shading is one standard deviation of 8 years of annual or seasonal means for the MG2 simulation. ANN = annual; DJF = December–February; JJA = June–August; PRISM = Parameter-elevation Relationships on Independent Slopes Model.

United States is available at 4-km resolution (Daly et al., 2008). Here it has been regridded to 12 km for better comparison to the 14-km high-resolution simulations. Figure 11 illustrates biases in MG2 against the PRISM precipitation data set, showing significantly lower precipitation in the coastal ranges in winter (Figure 11a), with excess precipitation in the Northeast United States. In summer (Figure 11b), the largest biases are over the Rocky Mountains.

Next we examine the impact of rimed ice (graupel) on precipitation. There is a small impact of graupel seen in climatologies over CONUS, even at high resolution (Figures 8 and 10). Coherent impacts show up only in surface precipitation field. Figure 12a illustrates the difference between annual total (stratiform and convective) precipitation in MG3 and MG2 based on two 8-year simulations. Total precipitation is analyzed to facilitate comparison to observations (see below). The picture for stratiform precipitation looks very similar. Only shown are differences which are statistically different than zero based on a 5–95% confidence interval of a bootstrap sampling with 1,000 samples. Bootstrap sampling was chosen to provide the best measure of significance for small samples with an unknown distribution of differences. In the Cascade range of the N.W. United States, there is a significant change in precipitation between the two simulations in the annual mean (Figure 12a) which occurs mostly during summer (JJA, Figure 12c). This represents an improvement of a low precipitation bias in this region (Figure 11a) although the changes occur during summer and most bias is in winter. The significant summer decrease over Colorado (Figure 12c) is also an improvement over MG2 (Figure 11b), though most biases are north and south of this region (Figure 11b).

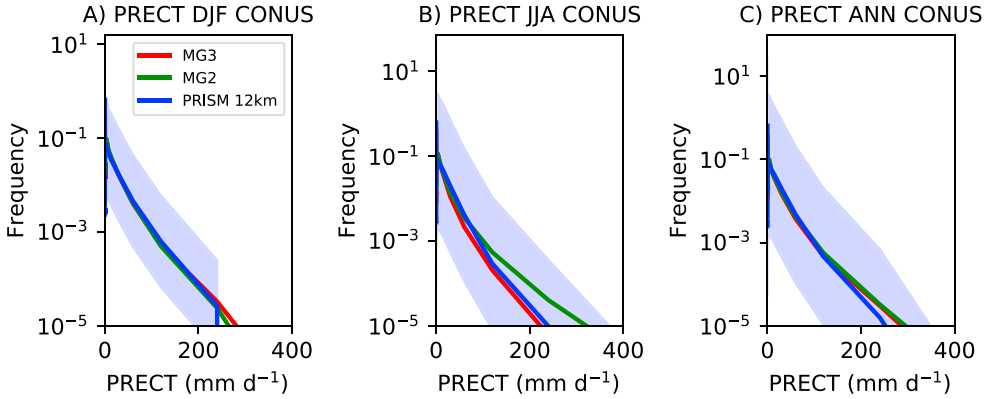

Figure 14. (a) Winter (DJF), (b) summer (JJA), and (c) ANN frequency of precipitation intensity over the United States for the simulations (red = MG3; green = MG2) and the PRISM data at 12 km (blue). Shaded area shows the monthly standard deviation from the PRISM data (log space). ANN = annual; DJF = December–February; JJA = June–August; PRISM = Parameter-elevation Relationships on Independent Slopes Model.

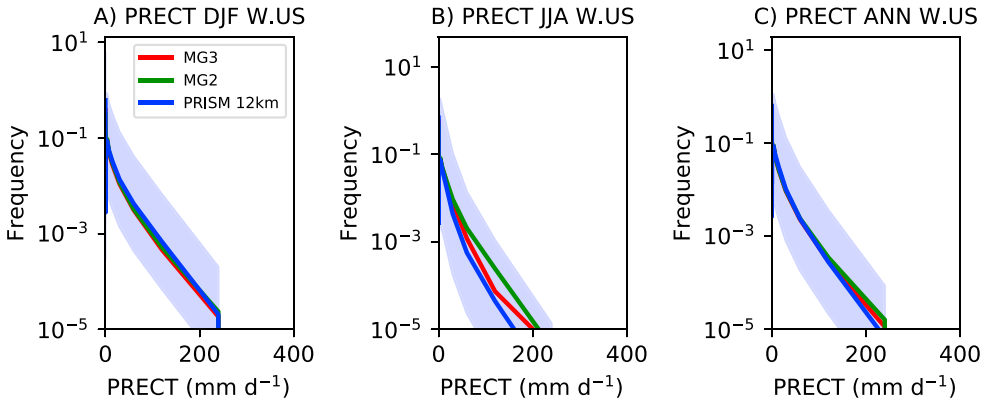

Figure 15. (a) Winter (DJF), (b) summer (JJA), and (c) ANN frequency of precipitation intensity over the Western United States (25–50° N, 105–130° W) for the simulations (red = MG3; green = MG2) and the PRISM data at 12 km (blue). Shaded area shows the monthly standard deviation from the PRISM data (calculated in log space). ANN = annual; DJF = December–February; JJA = June–August; PRISM = Parameter-elevation Relationships on Independent Slopes Model.

Figure 13 illustrates the average total precipitation over latitudes 38–48° N (from Colorado to Canada) along longitudes from the Pacific to Atlantic coast. Total precipitation (stratiform + convective) is analyzed because we are comparing to observations of total precipitation. The shading indicates one standard deviation σ from the MG2 simulation, indicating that a 2σ confidence interval is larger than most of the differences. Note also that the scale on each panel of Figure 13 is different, with more precipitation in winter (December–February, Figure 13b) than summer (JJA, Figure 13c). The comparison to PRISM indicates a slight increase in annual average precipitation in MG3 versus MG2 over the Western mountains. There is a seasonal shift in precipitation between MG3 and MG2 with decreases in MG3 (relative to MG2) during winter (Figure 13c) and increases in MG3 relative to MG2 during summer (Figure 13c). Half of the summer precipitation in the simulations is convective precipitation. Reductions in anomalous precipitation over the Rockies (105° W) are seen in MG3 relative to MG2 during summer (Figure 13c). On balance, the simulations show very little difference in precipitation between MG3 and MG2 (consistent with Figure 12), but a small improvement in MG3 for orographic precipitation regions of the Western United States (reducing a high bias in precipitation when averaged over 38–48° N).

Figure 14 illustrates seasonal and annual frequencies of precipitation intensity for the simulations and the PRISM data (at 12 km) using 5 years of PRISM data and 5 years from the simulations. PRISM data at 4 km have essentially the same frequency distribution. Simulations agree well with the PRISM data and are well within the variability of monthly frequency over the 5-year record in each bin. Winter (Figure 14a) precipitation intensities are very similar to PRISM observations. Summer precipitation intensities are lower in MG3 than MG2 and better in line with PRISM observations (Figure 14b). Annual frequency distributions for precipitation greater than 200 mm/day is higher in both MG3 and MG2 than PRISM data.

Figure 15 illustrates the precipitation intensity over the Western United States where some of the largest changes in precipitation occur (Figure 12). Consistent with the CONUS results in Figure 14, there is lower MG3 intensity than MG2 in JJA (Figure 15b) which carries through to annual results (Figure 15c), indicating slightly reduced intensities of precipitation with graupel. However, both model simulations do a good job of simulating precipitation intensity at 14 km and are well within the spread of observed variability.

Note that the mean precipitation (Figures 12 and 13) and precipitation intensity (Figures 14 and 15) are not directly comparable, since the mean is dominated by the higher frequency of more moderate or low precipitation events, which appear similar on the log scale of Figures 14 and 15.

7. Discussion/Conclusions

This work describes the implementation of rimed ice hydrometeors in a two-moment microphysics scheme (MG3) in a GCM used for climate studies (CAM6). Hail or graupel are selected based on density and fall speed parameters. MG3 is capable of producing reasonable solutions across a wide range of scales, which we have illustrated with a model hierarchy. We show MG3 forced with deep convective updraft strengths

(KiD), grid-scale forcing at 14 km, and weak stratiform grid-scale forcing at 100-km scale in both single column and global tests. The scheme produces regional climate simulations with acceptable graupel sizes and reasonable distributions, mostly related to strong orographic forcing of stratiform clouds.

Idealized simulations (KiD) indicate that MG3 is similar to other microphysical schemes commonly used in mesoscale models when forced with resolved scale updrafts (up to 16 m/s). The addition of rimed ice in MG3 causes a significant decrease in snow at altitudes above the melting level compared to the original scheme (MG2). This transformation impacts the timing of precipitation, as snow has a slower fall speed than rimed ice, and consequently, the inclusion of rimed ice increases the fall speed and the flux of precipitation and causes it to fall significantly earlier in MG3 over MG2. MG3 in this respect looks like other schemes with rimed hydrometeors.

We have performed global simulations to understand the impact of rimed ice with MG3. At 100-km (1°) resolutions typical of standard climate models, the addition of rimed ice results in small amounts of rimed ice in expected regions near the freezing level. But the mass is small, and rimed ice has a limited global impact on climate when run at 100-km horizontal resolution. There are impacts on the structure of snow and small impacts on high-level cloudiness due to rimed ice (graupel).

We also performed simulations with MG2 and MG3 using a refined mesh down to 14 km, which is more typical of regional climate models. When run at the higher horizontal resolution (14 km), MG3 produces realistic sizes and fall speeds for graupel and reasonable seasonal shifts in rimed hydrometeor production regions from winter orographic precipitation in the Western United States to episodic systems in the East and Southeast United States. Differences in total precipitation between MG3 and MG2 are generally not statistically significant at 14 km. The addition of rimed ice in MG3 at high resolution slightly increases orographic precipitation in the Cascade mountains of the Western United States where MG3 indicates significant near surface graupel and decreases total precipitation over the Rockies. This reduces MG2 model biases in precipitation relative to the PRISM data set. The changes from MG2 to MG3 are consistent with the idealized KiD simulations that show MG3 has an earlier onset of precipitation and slight increases. Previous work using mesoscale models also indicates orographic precipitation in the Western United States is sensitive to rimed ice (Morrison et al., 2015). Daily precipitation intensity for both MG2 and MG3 (the latter with graupel) is similar to PRISM observations. MG3 has reduced precipitation intensity for extreme events in summer, in better agreement with PRISM observations than MG2.

As expected, overall, there is little climate impact of rimed ice at typical (100 km) resolutions for global models, but important regional effects appear at higher resolution (14 km). Thus, regional climate simulations, particularly where there is orographic forcing, may see smaller-scale climate effects from rimed ice.

Note that these simulations include rimed ice only in the large-scale or stratiform microphysics, which in CAM6 is used for large-scale and shallow cumulus clouds that are created by the unified moist turbulence scheme (CLUBB). There is only a very simple parameterization of microphysics (a simple autoconversion scheme) in the deep convection scheme in CAM6 (Zhang & McFarlane, 1995). This is typical of most GCMs. Recent work (Song & Zhang, 2011; Song et al., 2012) has explored the use of a more detailed microphysics scheme driven by deep convective updrafts based on the original Morrison and Gettelman (2008) scheme. Future work will explore the addition of rimed hydrometeors in deep convection, where they would be expected to have larger and more significant impacts. This could be accomplished by a similar method to Song and Zhang (2011), extracting vertical velocities to drive the scheme, or it could be done with a more unified scheme by extending CLUBB to handle all types of clouds, following Thayer-Calder et al. (2015) and simply turning off the deep convective scheme. It is hypothesized that turning off the deep convective scheme will show even larger graupel effects on regional climate, particularly in regions dominated by continental convection.

The long-term goal is to unify microphysics and convection/turbulence treatments in models to be able to use models across multiple scales. Simulations here are conducted with idealized small scale updrafts that necessitate inclusion of rimed ice that could be either graupel or hail and with regional climate tests at 14 km, where rimed ice is likely mostly graupel. However, with the growing sophistication of variable-resolution

global models, we anticipate reaching nonhydrostatic storm scale resolutions (e.g., 1 km) in the near future, where hail parameters may be more appropriate. This work is a step in that direction, with some important implications for regional climate.

Appendix A: Budget Equations

Equations for all the prognostic variables in MG3 are given here for completeness. Equations (1) and (2) are for rimed ice (graupel or hail) and mass and number mixing ratios. The other vapor (Q_v), temperature (T), and cloud hydrometeor mass (Q) and number (N) mixing ratios are shown here. The fraction of the grid box (f) covered by precipitation (f_p), ice (f_i), and liquid condensate (f_c) also appears in the equations. *xls* is the latent heat of sublimation, *xlf* the latent heat of freezing, and *xlv* the laten heat of vaporization.

$$\frac{dQ_v}{dt} = (PRE + PRDS) \times f_p - VAPDEP - ISUBLIM - MNUCCD - MNUDEP \times f_c - (PRDG + EPRDG) \times f_p. \tag{A1}$$

$$\begin{aligned}\frac{dT}{dt} = {} & [(PRE \times f_c) \times xlv \\ & + (PRDS + PRDG) \times f_c + VAPDEP + ISUBLIM + MNUCCD + MNUDEP f_c] \times xls \\ & + [(BERGS + PSACWS + MNUCCC + MNUCCT + MSACWI + PSACWG + QMULTG + PGSACW) \times f_c \\ & + (MNUCCR + PRACS + MNUCCRI + PRACG + PGRACS + QMULTRG) f_p + BERG] \times xlf.\end{aligned} \tag{A2}$$

$$\frac{dQ_c}{dt} = (-PRA - PRC - MNUCCC - MNUCCT - MSCAWI - PSACWS - BERGS - QMULTG - PSACWG - PGSACW) \times f_c - BERG. \tag{A3}$$

$$\begin{aligned}\frac{dQ_i}{dt} = {} & (MNUCCC + MNUCCT + MNUDEP + MSACWI) \times f_c \\ & + (-PRCI - PRAI) f_i + VAPDEP + BERG + ISUBLIM \\ & + QMULTG \times f_c + QMULTRG \times f_p + MNUCCD + MNUCCRI \times f_p.\end{aligned} \tag{A4}$$

$$\frac{dQ_r}{dt} = (PRA + PRC) \times f_c + (PRE - PRACS - MNUCCR - MNUCCRI - QMULTRG - PRACG - PGRACS) \times f_p. \tag{A5}$$

$$\frac{dQ_s}{dt} = (PRAI + PRCI) f_i + (PSACWS + BERGS) \times f_c + (PRDS + PRACS + MNUCCR - PSACR) \times f_p. \tag{A6}$$

$$\frac{dN_c}{dt} = (-NNUCCC - NNUCCT - NPSACWS + - NPRA - NPRC - NPSACWG) \times f_c. \tag{A7}$$

$$\frac{dN_i}{dt} = NNUCCD + (NNUCCT + NNUCCC + NNUDEP + NSACWI + NMULTG) \times f_c + (NSUBI - NPRCI - NPRAI) \times f_i + (NMULTRG + NNUCCRI) \times f_p. \tag{A8}$$

$$\frac{dN_r}{dt} = NPRC \times f_c + (NSUBR - NPRACS - NNUCCR - NNUCCRI + NRAGG - NPRACG - NGRACS) \times f_p. \tag{A9}$$

Table A1
MG3 Microphysical Processes

Q Process	N Process	Description	Fraction
PRA	NPRA	Accretion of liquid to rain	Cloud
PRC	NPRC	Liquid autoconversion	Cloud
PRCI	NPRCI	Accretion of ice to snow	Cloud
PRAI	NPRAI	Ice autoconversion	Cloud
PRE	NSUBR	Rain evaporation	Precip
PRDS	NSUBS	Snow evaporation	Precip
VAPDEP		Vapor deposition to ice	
ISUBLIM	NSUBI	Sublimation from ice to vapor	
MNUCCD	NNUCCD	Ice nucleation from deposition/condensation freezing	
MNUDEP	NNUDEP	Deposition nucleation (mixed phase clouds)	Cloud
BERGS		Bergeron process (drops) onto snow	Cloud
PSACWS	NPSACWS	Collection of drops by snow	Cloud
MNUCCC	NNUCCC	Homogeneous freezing of drops	Cloud
MNUCCT	NNUCCT	Contact freezing of drops	Cloud
MSACWI	NSACWI	Ice multiplication	Cloud
MNUCCR	NNUCCR	Rain freezing	Precip
PRACS	NPRACS	Collection of rain by snow	Precip
MNUCCRI	NNUCCRI	Freezing of rain to ice	Precip
	NSAGG	Snow aggreagation process	Precip
BERG		Bergeron process (drops) onto ice	
*PSACR		Collection snow → rain	Precip
*PRACG	NPRACG	Rain collection → graupel	Precip
*PSACWG	NPSACWG	Drop collection → graupel	Cloud
*PGSACW	NSCNG	Drop → graupel due to droplet collection on snow	Cloud
*PGRACS	NGRACS	Rain → graupel to rain collection on snow	Precip
*PRDG		Graupel deposition	Precip
*EPRDG		Graupel sublimation	Precip
*QMULTG	NMULTG	Ice multiplication drops → graupel	Cloud
*QMULTRG	NMULTRG	Ice multiplication rain → graupel	Precip

Note. New processes are identified with an asterisk.

$$\frac{\mathrm{d}N_\mathrm{s}}{\mathrm{d}t} = (NSUBS + NSAGG + NNUCCR - NGRACS) \times f_\mathrm{p} + (NPRCI - NSCNG) \times f_\mathrm{i}. \tag{A10}$$

Table A1 presents a list of process rates in the equations above. A detailed description of the rates is contained in Morrison and Gettelman (2008) and Gettelman and Morrison (2015). Those marked with asterisks (∗) are described in Table 1.

Acknowledgments
MG3 model code is available in public repositories for the Community Earth System Model upon release or by developer agreement before release. Model output for particular simulations in this manuscript and most importantly the MG3 code is available online (ftp://ftp.cgd.ucar.edu/archive/andrew/mg3). The National Center for Atmospheric Research is supported by the United States National Science Foundation. Variable resolution simulations were performed with support from the Computational and Information Sciences Laboratory (CISL) Accelerated Science Discovery project. This work was partially supported by NASA grant 80NSSC17K0073.

References

Adams-Selin, R. D., van den Heever, S. C., & Johnson, R. H. (2013). Impact of graupel parameterization schemes on idealized bow echo simulations. *Monthly Weather Review*, *141*(4), 1241–1262. https://doi.org/10.1175/MWR-D-12-00064.1

Bogenschutz, P. A., Gettelman, A., Morrison, H., Larson, V. E., Craig, C., & Schanen, D. P. (2013). Higher-order turbulence closure and its impact on climate simulation in the Community Atmosphere Model. *Journal of Climate*, *26*(23), 9655–9676. https://doi.org/10.1175/JCLI-D-13-00075.1

Brown, A., Milton, S., Cullen, M., Golding, B., Mitchell, J., & Shelly, A. (2012). Unified modeling and prediction of weather and climate: A 25-year journey. *Bulletin of the American Meteorological Society*, *93*(12), 1865–1877. https://doi.org/10.1175/BAMS-D-12-00018.1

Bryan, G. H., & Morrison, H. (2012). Sensitivity of a simulated squall line to horizontal resolution and parameterization of microphysics. *Monthly Weather Review*, *140*(1), 202–225. https://doi.org/10.1175/MWR-D-11-00046.1

Colle, B. A., Garvert, M. F., Wolfe, J. B., Mass, C. F., & Woods, C. P. (2005). The 13–14 December 2001 IMPROVE-2 event. Part III: Simulated microphysical budgets and sensitivity studies. *Journal of the Atmospheric Sciences*, *62*(10), 3535–3558. https://doi.org/10.1175/JAS3552.1

Colle, B. A., Lin, Y., Medina, S., & Smull, B. F. (2008). Orographic modification of convection and flow kinematics by the Oregon Coast Range and Cascades during IMPROVE-2. *Monthly Weather Review*, *136*(10), 3894–3916. https://doi.org/10.1175/2008MWR2369.1

Cooper, W. A. (1986). Ice initiation in natural clouds. Precipitation enhancement—A scientific challenge. *Meteorological Monographs*, *43*, 29–32.

Daly, C., Halbleib, M., Smith, J. I., Gibson, W. P., Doggett, M. K., Taylor, G. H., et al. (2008). Physiographically sensitive mapping of climatological temperature and precipitation across the Conterminous United States. *International Journal of Climatology*, *28*(15), 2031–2064. https://doi.org/10.1002/joc.1688

Ferrier, B. (1994). A double-moment multiple-phase four-class bulk ice scheme. Part I: Description. *The Journal of Asian Studies*, *51*, 249–280.

Gettelman, A., Callaghan, P., Larson, V. E., Zarzycki, C. M., Bacmeister, J. T., Lauritzen, P. H., et al. (2018). Regional climate simulations With the Community Earth System Model. *Journal of Advances in Modeling Earth Systems*, *10*, 1245–1265. https://doi.org/10.1002/2017MS001227

Gettelman, A., & Morrison, H. (2015). Advanced two-moment bulk microphysics for global models. Part I: Off-line tests and comparison with other schemes. *Journal of Climate*, *28*(3), 1268–1287. https://doi.org/10.1175/JCLI-D-14-00102.1

Gettelman, A., Morrison, H., Santos, S., Bogenschutz, P., & Caldwell, P. M. (2015). Advanced two-moment bulk microphysics for global models. Part II: Global model solutions and aerosol-cloud interactions. *Journal Climate*, *28*(3), 1288–1307. https://doi.org/10.1175/JCLI-D-14-00103.1

Gettelman, A., Truesdale, J. E., Bacmeister, J. T., Caldwell, P. M., Neale, R. B., Bogenschutz, P. A., & Simpson, I. R. (2019). The Single Column Atmosphere Model version 6 (SCAM6): Not a scam but a tool for model evaluation and development. *Journal of Advances in Modeling Earth Systems*, *11*. https://doi.org/10.1029/2018MS001578

Golaz, J.-C., Larson, V. E., & Cotton, W. R. (2002). A PDF-based model for boundary layer clouds. Part II: Model results. *Journal of the Atmospheric Sciences*, *59*, 3552–3571.

Guba, O., Taylor, M. A., Ullrich, P. A., Overfelt, J. R., & Levy, M. N. (2014). The spectral element method (SEM) on variable-resolution grids: Evaluating grid sensitivity and resolution-aware numerical viscosity. *Geoscientific Model Development*, *7*(6), 2803–2816. https://doi.org/10.5194/gmd-7-2803-2014

Heymsfield, A. J., Bansemer, A., & Twohy, C. H. (2007). Refinements to ice particle mass dimensional and terminal velocity relationships for ice clouds. Part I: Temperature dependence. *Journal of the Atmospheric Sciences*, *64*(4), 1047–1067. https://doi.org/10.1175/JAS3890.1

Heymsfield, A. J., & Donner, L. J. (1990). A scheme for parameterizing ice-cloud water content in general circulation models. *The Journal of Asian Studies*, *47*(15), 1865–1877.

Huang, X., Rhoades, A. M., Ullrich, P. A., & Zarzycki, C. M. (2016). An evaluation of the variable-resolution CESM for modeling California's climate. *Journal of Advances in Modeling Earth Systems*, *8*, 345–369. https://doi.org/10.1002/2015MS000559

Ikawa, M., & Saito, K. (1990). Description of the nonhydrostatic model developed at the Forecast Research Department of the MRI. Tech. Rep. 28, Meteorological Institute MRI.

Larson, V. E., Golaz, J.-C., & Cotton, W. R. (2002). Small-scale and mesoscale variability in cloudy boundary layers: Joint probability density functions. *Journal of the Atmospheric Sciences*, *59*(24), 3519–3539. https://doi.org/10.1175/1520-0469(2002)059<3519:SSAMVI>2.0.CO;2

Lim, K.-S. S., & Hong, S.-Y. (2010). Development of an effective double-moment cloud microphysics scheme with prognostic cloud condensation nuclei (CCN) for weather and climate models. *Monthly Weather Review*, *138*(5), 1587–1612. https://doi.org/10.1175/2009MWR2968.1

Lin, Y., & Colle, B. A. (2011). A new bulk microphysical scheme that includes riming intensity and temperature-dependent ice characteristics. *Monthly Weather Review*, *139*(3), 1013–1035. https://doi.org/10.1175/2010MWR3293.1

Lin, Y., Donner, L. J., & Colle, B. A. (2011). Parameterization of riming intensity and its impact on ice fall speed using ARM data. *Monthly Weather Review*, *139*(3), 1036–1047. https://doi.org/10.1175/2010MWR3299.1

Locatelli, J. D., & Hobbs, P. V. (1974). Fall speeds and masses of solid precipitation particles. *Journal of Geophysical Research*, *79*, 2185–2197. https://doi.org/10.1029/JC079i015p02185

Lohmann, U., Feichter, J., Chuang, C. C., & Penner, J. (1999). Prediction of the number of cloud droplets in the ECHAM GCM. *Journal of Geophysical Research*, *104*(D8), 9169–9198.

Matson, R. J., & Huggins, A. W. (1980). The direct measurement of the sizes, shapes and kinematics of falling hailstones. *Journal of the Atmospheric Sciences*, *37*(5), 1107–1125. https://doi.org/10.1175/1520-0469(1980)037<1107:TDMOTS>2.0.CO;2

McCumber, M., Tao, W.-K., Simpson, J., Penc, R., & Soong, S.-T. (1991). Comparison of ice-phase microphysical parameterization schemes using numerical simulations of tropical convection. *Journal of Applied Meteorology*, *30*(7), 985–1004. https://doi.org/10.1175/1520-0450-30.7.985

Milbrandt, J. A., & Yau, M. K. (2005). A multimoment bulk microphysics parameterization. Part I: Analysis of the role of the spectral shape parameter. *Journal of the Atmospheric Sciences*, *62*(9), 3051–3064. https://doi.org/10.1175/JAS3534.1

Morrison, H., Curry, J. A., & Khvorostyanov, V. I. (2005). A new double-moment microphysics parameterization for application in cloud and climate models. Part I: Description. *The Journal of Asian Studies*, *62*, 1665–1677.

Morrison, H., & Gettelman, A. (2008). A new two-moment bulk stratiform cloud microphysics scheme in the NCAR Community Atmosphere Model (CAM3), Part I: Description and numerical tests. *Journal of Climate*, *21*(15), 3642–3659.

Morrison, H., Milbrandt, J. A., Bryan, G. H., Ikeda, K., Tessendorf, S. A., & Thompson, G. (2015). Parameterization of cloud microphysics based on the prediction of bulk ice particle properties. Part II: Case study comparisons with observations and other schemes. *Journal of the Atmospheric Sciences*, *72*(1), 312–339. https://doi.org/10.1175/JAS-D-14-0066.1

Morrison, H., Thompson, G., & Tatarskii, V. (2009). Impact of cloud microphysics on the development of trailing stratiform precipitation in a simulated squall line: Comparison of one- and two-moment schemes. *Monthly Weather Review*, *137*, 991–1007. https://doi.org/10.1175/2008MWR2556.1

Murakami, M. (1990). Numerical modeling of dynamical and microphysical evolution of an isolated convective cloud. *Journal of the Meteorological Society of Japan. Ser. II*, *68*(2), 107–128. https://doi.org/10.2151/jmsj1965.68.2.107

Rauscher, S. A., Ringler, T. D., Skamarock, W. C., & Mirin, A. A. (2012). Exploring a global multiresolution modeling approach using aquaplanet simulations. *Journal of Climate*, *26*(8), 2432–2452. https://doi.org/10.1175/JCLI-D-12-00154.1

Reisner, J., Rasmussen, R., & Bruintjes, R. T. (1998). Explicit forecasting of supercooled liquid water in winter storms using the MM5, forecast model. *Quarterly Journal of the Royal Meteorological Society*, *124*, 1071–1107.

Rutledge, S. A., & Hobbs, P. V. (1984). The mesoscale and microscale structure and organization of clouds and precipitation in midlatitude cyclones. XII: A diagnostic modeling study of precipitation development in narrow cold-frontal rainbands. *Journal of the Atmospheric Sciences*, *41*(20), 2949–2972. https://doi.org/10.1175/1520-0469(1984)041<2949:TMAMSA>2.0.CO;2

Seifert, A., & Beheng, K. D. (2006). A two-moment cloud microphysics parameterization for mixed-phase clouds. Part 1: Model description. *Meteorology and Atmospheric Physics*, *92*(1), 45–66. https://doi.org/10.1007/s00703-005-0112-4

Shipway, B. J., & Abel, S. J. (2010). Analytical estimation of cloud droplet nucleation based on an underlying aerosol population. *Atmospheric Research*, *96*(2), 344–355. https://doi.org/10.1016/j.atmosres.2009.10.005

Shipway, B. J., & Hill, A. A. (2011). The Kinematic Driver model (KiD). Technical Report 549, U.K. Met Office.

Shipway, B. J., & Hill, A. A. (2012). Diagnosis of systematic differences between multiple parametrizations of warm rain microphysics using a kinematic framework. *Quarterly Journal of the Royal Meteorological Society*, *138*(669), 2196–2211. https://doi.org/10.1002/qj.1913

Song, X., & Zhang, G. J. (2011). Microphysics parameterization for convective clouds in a global climate model: Description and single column model tests. *Journal of Geophysical Research*, *116*, D02201. https://doi.org/10.1029/2010JD014833

Song, X., Zhang, G. J., & Li, J. L. F. (2012). Evaluation of microphysics parameterization for convective clouds in the NCAR Community Atmosphere Mode CAM5. *Journal of Climate*, *25*(24), 8568–8590. https://doi.org/10.1175/JCLI-D-11-00563.1

Taylor, M. A. (2011). Conservation of mass and energy for the moist atmospheric primitive equations on unstructured grids. In P. Lauritzen, C. Jablonowski, M. Taylor, & R. Nair (Eds.), *Numerical techniques for global atmospheric models, Lecture Noted in Computational Science and Engineering* (Vol. 80, pp. 357–380). Berlin Heidelberg: Springer. https://doi.org/10.1007/978-3-642-11640-7-12

Thayer-Calder, K., Gettelman, A., Craig, C., Goldhaber, S., Bogenschutz, P. A., Chen, C.-C., et al. (2015). A unified parameterization of clouds and turbulence using CLUBB and subcolumns in the Community Atmosphere Model. *Geoscientific Model Development*, *8*(12), 3801–3821. https://doi.org/10.5194/gmd-8-3801-2015

Thompson, G., Field, P. R., Rasmussen, R. M., & Hall, W. D. (2008). Explicit forecasts of winter precipitation using an improved bulk microphysics scheme. Part II: Implementation of a new snow parameterization. *Monthly Weather Review*, *136*(12), 5095–5115. https://doi.org/10.1175/2008MWR2387.1

Van Weverberg, K., Vogelmann, A. M., Morrison, H., & Milbrandt, J. A. (2012). Sensitivity of idealized squall-line simulations to the level of complexity used in two-moment bulk microphysics schemes. *Monthly Weather Review*, *140*(6), 1883–1907. https://doi.org/10.1175/MWR-D-11-00120.1

van den Heever, S. C., & Cotton, W. R. (2004). The impact of hail size on simulated supercell storms. *Journal of the Atmospheric Sciences*, *61*(13), 1596–1609. https://doi.org/10.1175/1520-0469(2004)061<1596:TIOHSO>2.0.CO;2

Wu, D., Dong, X., Xi, B., Feng, Z., Kennedy, A., Mullendore, G., et al. (2013). Impacts of microphysical scheme on convective and stratiform characteristics in two high precipitation squall line events. *Journal of Geophysical Research: Atmospheres*, *118*, 11,119–11,135. https://doi.org/10.1002/jgrd.50798

Zarzycki, C. M., & Jablonowski, C. (2014). A multidecadal simulation of Atlantic tropical cyclones using a variable-resolution global atmospheric general circulation model. *Journal of Advances in Modeling Earth Systems*, *6*, 805–828. https://doi.org/10.1002/2014MS000352

Zarzycki, C. M., Levy, M. N., Jablonowski, C., Overfelt, J. R., Taylor, M. A., & Ullrich, P. A. (2014). Aquaplanet experiments using CAM's variable-resolution dynamical core. *Journal of Climate*, *27*(14), 5481–5503. https://doi.org/10.1175/JCLI-D-14-00004.1

Zhang, G. J., & McFarlane, N. A. (1995). Sensitivity of climate simulations to the parameterization of cumulus convection in the Canadian Climate Center general circulation model. *Atmosphere-Ocean*, *33*, 407–446.